Organic Electronics 122 (2023) 106888

Contents lists available at ScienceDirect

Organic Electronics

journal homepage: www.elsevier.com/locate/orgel

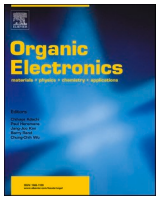

Measuring frontier orbital energy levels of OLED materials using cyclic voltammetry in solution

Gabriela P. Kissling [a], Beat Ruhstaller [a,b], Kurt P. Pernstich [a,*]

[a] Institute of Computational Physics, Zurich University of Applied Sciences ZHAW, 8401, Winterthur, Switzerland
[b] Fluxim AG, Katharina-Sulzer-Platz 2, 8400, Winterthur, Switzerland

A B S T R A C T

The operation of organic light emitting diodes (OLEDs) is governed by a range of material parameters, such as frontier orbital energy levels, charge carrier mobility and excitonic rate parameters. In state-of-the art numerical simulations of OLED devices, more than 30 parameters must be considered to describe the behavior of a multilayer device. Independent measurement techniques to reliably determine each material parameter individually are therefore highly desirable. While several techniques have been established in the OLED community to determine some of them, the highest occupied and lowest unoccupied molecular orbital (HOMO and LUMO) energy levels are not measured or reported on a regular basis, despite their significant influence on device performance. In this work, we show how cyclic voltammetry in solution can be used as a simple technique to measure the HOMO and LUMO energy levels of organic semiconductors. This easily performed experiment allows a fairly accurate estimation of the energy levels of the layers in a device stack. Cyclic voltammetry measurements of four typical OLED materials in solution are presented and their analysis is described in detail to encourage more such measurements in future OLED studies. Four distinctly different voltammograms were obtained, ranging from relatively ideal reversible behavior to a very non-ideal behavior, lacking electrochemical reverse reactions. Two methods for extracting the HOMO and LUMO energy levels from cyclic voltammetry are discussed and compared. The measured HOMO and LUMO levels compare well with reported values measured on thin films, showing that cyclic voltammetry in solution provides a viable means to determine this important, yet underinvestigated material property.

1. Introduction

Organic light emitting diodes (OLEDs) have been commercially established for the past 15–30 years [1]. Current research focuses on increasing OLED device efficiency and lifetime by developing new materials and improving device architectures through better understanding of the governing physical mechanisms. The ongoing optimization work is strongly supported by device simulations which help to understand the influence of various parameters on the device efficiency. To obtain high quality data from device simulations the accurate values for the model parameters are essential. After all, more than 30 parameters, such as charge carrier mobilities, energy levels, and trap and excitonic rate parameters are needed to simulate a device [2]. One particularly relevant set of parameters necessary for device simulations is the location of the HOMO and LUMO energy levels of the different device layers. As with all semiconductor devices, the alignment of each semiconductor layer's frontier energy levels (HOMOs and LUMOs) and of the electrode work functions has a significant impact on the device performance [3]. For instance, in the modified thermionic emission model [4] that can describe current injection from a metal to an adjacent organic semiconductor, the injection current density depends exponentially on the energy barrier ΔE between the metal work function and the corresponding frontier orbital energy level of the organic semiconductor. Charge transport between two organic semiconductors is often described by assuming quasi-Fermi level alignment, thus, the charge carrier density in adjacent layers is determined by the Fermi statistics, where the charge carrier density also depends exponentially on the energetic offset between the frontier orbital energy levels of adjacent layers. Therefore, even small changes in the HOMO and LUMO levels can have a profound impact on the device performance and, thus, should be independently and accurately measured to obtain a reliable device model. The importance of reporting HOMO/LUMO levels on a regular basis has been underlined by Jeong and coworkers [5] who trained a deep learning model with the HOMO and LUMO levels of different organic molecules to design new host and emitter materials for OLEDs.

There are various methods to determine HOMO and LUMO energy levels. All have their advantages and disadvantages. In this paper we will give a brief overview and then describe in detail how to determine frontier orbital energy levels using simple electrochemical methods. HOMO and LUMO energy levels of OLED materials can be theoretically

* Corresponding author.
E-mail address: kurt.pernstich@zhaw.ch (K.P. Pernstich).

https://doi.org/10.1016/j.orgel.2023.106888
Received 2 December 2022; Received in revised form 15 May 2023; Accepted 30 June 2023
Available online 1 July 2023

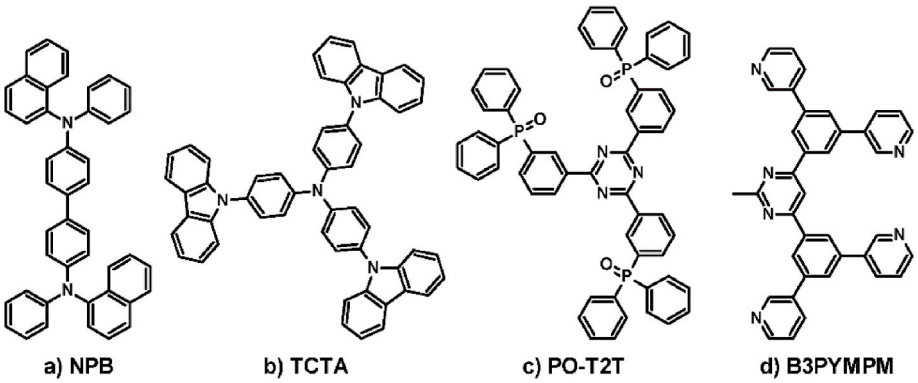

Fig. 1. Structures of the hole (a, b) and electron (c, d) transport materials discussed in this paper: N,N′-bis(naphthalen-1-yl)-N,N′-bis(phenyl)-benzidine (NPB) (a), 4,4′,4-tris(carbazol-9-yl)triphenylamine (TCTA) (b), 2,4,6-tris[3-(diphenylphosphinyl)phenyl]-1,3,5-triazine (PO-T2T) (c) and 4,6-bis(3,5-di(pyridin-3-yl)phenyl)-2-methylpyrimidine (B3PYMPM) (d).

predicted using density functional theory [6–8]. These works are mostly limited to a single molecule in a vacuum environment. Experimental methods to measure HOMO and LUMO energies include surface analysis techniques, such as XPS [9], UPS [10] and photoemission yield spectroscopy (PYS) [11–13], or inverse photoemission spectroscopy (IPES) [14,15], low-energy inverse photoemission spectroscopy [16,17] and Kelvin Probe spectroscopy [18]. Most recently, a method was described by Zhou et al. using a three-terminal hot-electron transistor [19]. Another method that allows probing of the HOMO and the LUMO is electrochemistry, although in most cases only one of the energy levels of a given molecule can be probed as the potential window of most electrolytes is not wide enough to access both frontier orbital energy levels.

Unfortunately, none of the techniques is regularly used and therefore the HOMO and LUMO levels are often estimated. The issue when using estimated HOMO and LUMO energy levels or values reported in literature is that they span a wide range. This might be due to systematic variations between different measurement techniques [20–23], or it may be sample dependent. In any case, a reliable method to determine the HOMO and LUMO levels on a regular basis is desirable, as it would allow individual labs to measure the energy levels themselves, rather than relying on parameter values reported in literature or provided by material suppliers. In return, the improvement in data could benefit device modelling and thus lead to improved OLEDs.

Since the exact location of the various HOMOs and LUMOs will be determined by their chemical environment it is expected that there will be a difference when a molecule is measured in solution or in a thin film. Hence, measuring frontier orbital energy levels in thin films would be desirable. A complicating factor in electrochemical experiments is the stability of OLED thin films in the solvent environments which are needed for electrochemical measurements. This is possibly one of the reasons why until now most electrochemical thin film characterization was performed on polymeric semiconductor materials, such as P3HT [24–28]. Only few electrochemical characterizations of small molecule thin films exist [29–31] and we did not find any reports on the electrochemical behavior of modern OLED materials in thin films. Our own preliminary work suggests that thin films of common small molecular semiconductors used in modern OLEDs are easily soluble in common solvents used as electrolyte during electrochemical characterization. Thus, applying conventional electrochemical methods to this important class of materials is challenging. In return, the solubility of common OLED materials in typical solvents used in electrochemistry is often sufficient to study the molecules well in solution. The electrochemical characterization of OLED materials in solution is simple and therefore electrochemical measurements are often used as the first method to determine the HOMO and LUMO energy levels of OLED materials [10,12,32–35].

While the clear disadvantage of electrochemical measurements of OLED materials in solution is the difference in chemical environment, we believe that there is still a benefit to these experiments as the energetic shift for each molecule when characterized in solution or as a thin film is expected to be similar. After all, the change in the dipolar environment should be comparable. Thus, while the electrochemical measurements in solution do not provide a direct measurement of the molecular energy levels within an OLED stack, the use of a single analysis method for all layer materials will provide a consistent set of data which should help minimize modelling errors.

Electrochemical characterization of OLED materials using cyclic voltammetry is not new, but the analysis of the data does pose some challenges which we want to address in this paper in order to encourage researchers to include measured energy levels in future reports of their work. We present two methods for the analysis of the cyclic voltammetry of OLED materials in solution using four well known OLED materials: N,N′-Bis(naphthalen-1-yl)-N,N′-bis(phenyl)-benzidine (NPB), 4,4′,4-Tris(carbazol-9-yl)triphenylamine (TCTA), 2,4,6-Tris[3-(diphenylphosphinyl)phenyl]-1,3,5-triazine (PO-T2T) and 4,6-Bis(3,5-di(pyridin-3-yl)phenyl)-2-methylpyrimidine (B3PYMPM). Sketches of the molecular structures of the different molecules are provided in Fig. 1.

This paper will give an overview over the existing characterization of these materials and provide a detailed experimental method to electrochemically measure frontier orbital energy levels, even if the cyclic voltagrams look complicated. Emphasis is laid on the detailed description of the conversion between the electrochemical potential scale and the vacuum energy scale to highlight the existing uncertainties and to suggest a data presentation method which will allow more easy comparison of experimental data in the future, especially for OLED materials from small molecules which are hard to analyze as thin films. The main text contains descriptions of how to extract the HOMO or LUMO energy levels from the electrochemical data and gives a detailed discussion about the conversion from the electrochemical potential scale to the vacuum energy scale. The electrochemical behavior of the four hole- and electron conductor materials shown in Fig. 1 is also presented and discussed in detail. The electronic supplementary information provides some additional electrochemical data and their analysis. We hope that this paper will provide a method and motivation to measure, analyze and present OLED material data for the community using a simple experimental framework.

1.1. Nomenclature

We provide a small electrochemistry nomenclature defining the most important electrochemical terms used in this report in intuitive order because some terms have been used in different ways in literature.

Working electrode: The electrode at which the electrochemical reaction is measured. The electrochemical reactions are generated through electron exchange between the working electrode and the redox species, which is in the electrode's immediate vicinity (within a few Å).

Redox species: The electrochemically active compound (material under test) dissolved in the electrolyte. It causes the measured oxidation and reduction currents. In the current publication, the redox species are the investigated OLED materials or ferrocene.

Counter electrode: An electrode used to close the electrical circuit with the working electrode. Often consisting of a metal mesh or wire. Ideally its active area is larger than the area of the working electrode.

Reference electrode: An electrode used by the potentiostat to define 0 V with respect to a separate electrochemical reaction (such as $AgCl + e^- \rightleftarrows Ag + Cl^-$) held at equilibrium. This electrochemical reaction occurs at the reference electrode. Common reference electrodes are the Ag/AgCl reference electrode, the saturated calomel electrode (SCE, Hg/Hg_2Cl_2) and the standard hydrogen electrode (SHE, $2\ H^+(aq) + 2\ e^- \rightleftarrows H_2(g)$).

Quasi reference electrode: A metal wire (Ag, Pt, …) used instead of a proper reference electrode for situations where the use of a reference electrode is not practical. Unlike the reference electrode, the absolute potential defined by the quasi-reference electrode is less well defined, but usually remains constant during an experiment. Ferrocene is often added to the system at the end of the experiment to provide an internal standard.

Electrolyte: The investigated solution, containing the solvent and the supporting electrolyte. The solvent and supporting electrolyte are chosen according to the solubility and stability of the material under test. We would like to note, that in the literature, the term electrolyte is sometimes defined in other ways: the electrolyte sometimes refers to the whole solution between the electrodes, including the material under test, and sometimes it refers to what we refer to as the supporting electrolyte.

Supporting electrolyte: An electrochemically inactive ionic species added to the electrolyte to increase its conductivity. Amounts of approximately 0.1 mol L^{-1} are generally used. A sufficient background conductivity is important in electrochemical measurements to ensure a good electrochemical behavior.

Oxidation: "Hole injection reaction". An electron is extracted from the investigated redox species ($X \rightarrow X^+ + e^-$) when it is in contact with an electrode surface at the appropriate potential (oxidation potential). The oxidation currents are shown as positive currents in the upper right quadrant of the plots with increasing potential plotted on the x-axis from left to right, according to IUPAC convention [36].

Reduction: "Electron injection reaction". An electron is injected into the investigated redox species ($X + e^- \rightarrow X^-$) when it is in contact with an electrode surface at the appropriate potential (reduction potential). The reduction currents are shown as negative currents in the lower left quadrant of the plots with decreasing potentials plotted on the x-axis from right to left according to IUPAC convention [36].

Reversible reaction: A reaction between the redox species and the electrode is said to be reversible, when the reaction kinetics at the electrode are sufficiently fast so that the surface concentration of the oxidized or reduced redox species (X^+ or X^-) follow the Nernst equation immediately. A convenient diagnostic for a reversible system is a separation of $56.5/n$ mV between the peak and the half-peak potential in a forward scan, where n is the number of electrons involved in the electrode reaction [37]. The peak potential is independent of the scan rate, and the separation of the oxidation and reduction peaks slightly depends on the potential where the voltage scan is reversed and is ≈57–59 mV at 25 °C for single electron transfer reactions at all scan rates [37]. The peak current is proportional to the square root of the scan rate and the ratio of oxidation and reduction peak currents remains constant, hence the transfer of charge in the oxidation reaction is exactly balanced in the reverse reduction reaction. Additionally, the oxidized or reduced redox species undergoes no chemical reaction and does not otherwise leave the system.

Quasi-reversible reaction: In quasi-reversible reactions, either the electron transfer between electrode and redox species is kinetically slow and the Nernstian equilibrium is not established immediately, or the oxidized or reduced redox species undergo chemical reactions or leave the system. In quasi-reversible systems, the shape of the voltammograms differ from reversible systems, and the peak separation between the oxidation and reduction peaks depends on the scan rate. The peak current in a quasi-reversible reaction is not proportional to the square root of the scan rate.

Potential: The potential at the working electrode measured against a nearby reference electrode. The potential of the reference electrode is chemically fixed and defined as 0 V.

Peak potential: The potential, at which the rate of the redox reaction is highest due to the balance of thermodynamic and kinetic parameters (diffusion rates and reaction rate), leading to a peak in the measured currents.

Half-peak potential: The potential, where the measured current is half of the current measured at peak potential.

Accessible potential window of the electrolyte: The potential range in which the electrolyte is electrochemically stable and does not react (e.g. degrade) at the working electrode. In this region, the electrolyte does not cause significant currents.

Ohmic region: A linear region in the voltammogram in which only the ohmic background current is measured; sometimes also called a "flat" region.

Anodic scan direction: Scanning the potential in cyclic voltammetry from negative to positive potential.

Cathodic scan direction: Scanning the potential in cyclic voltammetry from positive to negative potential.

Open-circuit potential: The open-circuit potential or open-circuit voltage is the electrochemical equilibrium potential of the system. It is defined by the electrode surface material, the electrolyte, and the redox species. The rate of the oxidation and reduction reactions are equal at the open-circuit potential such that the net current is zero. It must be noted that in many systems - the present ones included - the open-circuit potential [37] can drift with time. However, it still provides a good starting point for electrochemical measurements and can be measured directly with the potentiostat. Once the starting potential is chosen, the drift of the open-circuit potential is often ignored.

2. Experimental

All electrochemical experiments were performed in a Faraday cage placed inside a N_2 filled glove box. The O_2 and H_2O concentrations inside the box were kept below 50 ppm and 10 ppm, respectively.

2.1. Electrochemical setup

Cyclic voltammetry experiments were performed in a three-electrode cell (SVC-3, ALS Co. Ltd) using a BioLogic SP-300 potentiostat and the EC-Lab software package. A 1.6 mm diameter Pt disc working electrode (ALS Co. Ltd), a 0.5 mm diameter Pt wire counter electrode (Goodfellow, as drawn, 99.99+ %), and an 0.5 mm diameter Ag wire (Alfa Aesar, Premion®, 99.9985%) quasi reference electrode were used. The reference potential was calibrated using ferrocene (Fc) (Alfa Aesar, 99.5%) by adding a small amount (approx. 2–5 mg/10 mL) of ferrocene to the electrolyte at the end of the experiments and re-measuring the cyclic voltammetry experiments. Further details of how to define the reference potential vs. Fc are provided in section 3.1.

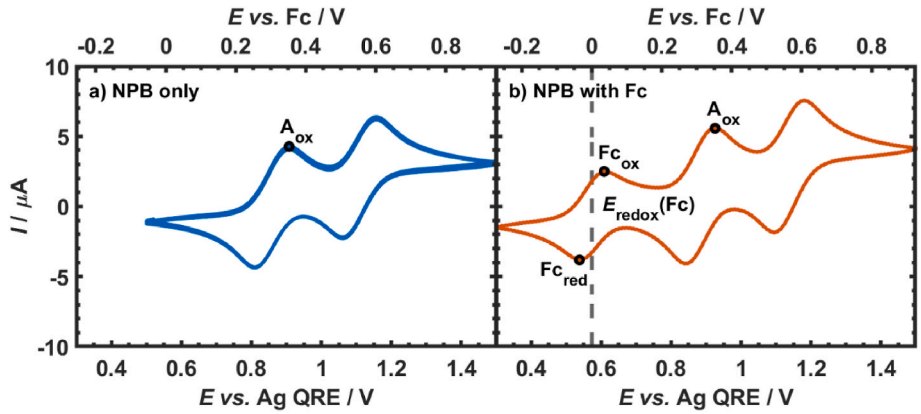

Fig. 2. Illustration of the potential conversion method. The CV of NPB was measured with respect to an Ag QRE (a). After the experiments, ferrocene was added to the electrolyte containing the NPB and the ferrocene redox potential was determined (b). The Fc redox potential was then defined as 0 V vs. Fc (see top x-axis in (b)) and a corresponding shift, including a potential shift due to handling the setup, was applied to the CV of NPB only (see top x-axis in (a)).

2.2. Electrode preparation

The electrodes were prepared outside the glove box. The Pt disc working electrode was first cleaned by wiping gently using low-lint tissue (Kimtech Precision Wipes) wetted with ultrapure water (resistivity of 18.2 MΩ cm), acetone or isopropanol and subsequently polished. Two grades of polishing suspensions (1 µm diamond suspension and 50 nm alumina suspension purchased including appropriate polishing cloths from ALS Co., Ltd.) were used. The polishing pads were stuck to the inside of separate Petri dishes and covered with the lid of the Petri dish when not used to avoid contamination. The Pt electrode was first polished using the 1 µm diamond suspension: 2–3 drops of the suspension were dropped on the polishing pad that was pre-wetted with a little bit of ultrapure water. The electrode was held perpendicularly to the surface of the pad and polished using gentle pressure and circle- or figure-of-eight movements for 2 min. The shaft of the electrode was rotated a little bit every 30 s to avoid introducing a slope into the electrode surface. The electrode was then rinsed with ultrapure water and the polishing procedure was repeated using the 50 nm alumina suspension. The electrode was rinsed again with ultrapure water and remains of the alumina suspension were removed from the electrode surface by wiping gently on a clean, wetted area of the polishing pad. After rinsing again with ultrapure water, the electrode was dried under a stream of nitrogen. The electrode surface now had a scratch-free mirror finish and the active surface was not touched anymore to avoid introduction of contaminants. Sonication of the electrode was omitted to prevent mechanical damage to the electrode. If the electrode surface is severely scratched for some reason, it may be necessary to resurface it more thoroughly by starting the polishing process using a coarser polishing agent (such as wetted lapping films or even wetted fine sandpaper).

The quasi reference and counter electrode wires were cleaned by wiping them with low-lint tissues wetted with first acetone and second isopropanol. Roughly 2 cm of each wire was immersed in the electrolyte for the electrochemical measurements.

2.3. Electrolyte preparation

Electrolytes were prepared inside the glove box. The electrolyte consisted of 0.1 mol L^{-1} tetrabutylammonium perchlorate (TBAP, Alfa Aesar, 99+ %) dissolved in dichloromethane (BDH, 99.8%, max. 0.001% H_2O). In addition, 1x10^{-3} mol L^{-1} of the investigated OLED material was added and all solids were left to dissolve at room temperature by stirring overnight with a magnetic stirrer bar. Dichloromethane was used as the solvent instead of the more common acetonitrile, as the solubility of the OLED materials (especially NPB [38]) was higher. NPB (sublimed, >99.8%), TCTA (sublimed, >99.5%), PO-T2T (sublimed, >99%) and B3PYMPM (sublimed, >99%) were obtained from Lumtec Corp. All compounds and solvents were used as received.

3. Analysis methods

3.1. Normalizing the electrochemical potential with respect to ferrocene

Obtaining a steady reference potential in non-aqueous electrolytes is a challenge, as existing reference electrodes for non-aqueous solvents [39] tend to be less stable as aqueous reference electrodes due to solvent evaporation. This also makes their maintenance challenging. Therefore, to avoid inconsistencies when reporting potentials in non-aqueous systems, it is advised to convert the measured potentials to the ferrocene reference scale, by measuring the redox potential of ferrocene and defining it as 0 V [40]. This is achieved by adding a small amount (a "pinch" or roughly 1 mmol L^{-1}) of ferrocene to the investigated electrolyte containing the material under test, dissolving it, and re-measuring the cyclic voltammetry. The potential scale of the cyclic voltammograms (CVs) is then shifted to set the redox potential of ferrocene to 0 V. The same shift, slightly adjusted to account for potential shifts during addition of the ferrocene due to handling of the setup, can then be applied to CVs measured without ferrocene. This process is illustrated in Fig. 2 and discussed in more detail below.

First, the material under test is electrochemically characterized (see Fig. 2a, bottom potential scale). In the present case, the oxidation potential of NPB was determined to be $A_{ox}^{Ag\ QRE} = 0.908$ V against the Ag wire quasi reference electrode (Ag QRE); the experimental data shown will be thoroughly discussed in section 4.1.1.

As a next step, ferrocene is added to the electrolyte containing the material under test (see Fig. 2b, bottom potential scale). Since the shape of the NPB peaks does not change, we can conclude that the presence of ferrocene does not affect the electrochemical behavior of NPB. Thus, A_{ox} can be re-measured in the presence of Fc and used to determine the potential shift due to handling the setup as discussed below. From Equation (1), the redox potential of ferrocene is determined to be $E_{redox}^{Ag\ QRE} = 0.573$ V.

$$E_{redox}^{Ag\ QRE}(Fc) = \frac{Fc_{red} + Fc_{ox}}{2} \quad \text{Equation 1}$$

Now, the potential scale is shifted by −0.573 V, as described in Equation (2), to achieve $E_{redox}^{Fc}(Fc) = 0\ V$. The shifted potential scale is shown in the top axis of Fig. 2b.

$$E_{NPB\ and\ Fc}^{Fc} = E^{Ag\ QRE} - E_{redox}^{Ag\ QRE}(Fc) \quad \text{Equation 2}$$

Before transferring the shifted potential scale to the NPB only CV

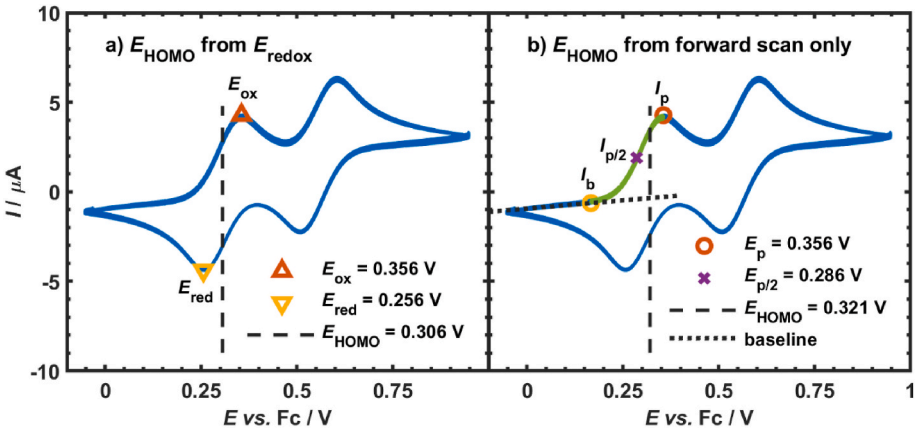

Fig. 3. CVs *of NPB measured at* 100 mV/s *to illustrate the determination of the HOMO from either the redox potential (a) or from the forward peak only (b). The dotted line in (b) accounts for the resistive losses in the electrolyte and is used to determine* I_p *and* $I_{p/2}$ if the peak to be analyzed is nicely resolved. For other systems, I_b can be chosen by eye to determine the peak- and half-peak currents required to determine the half-peak potential $E_{p/2}$.

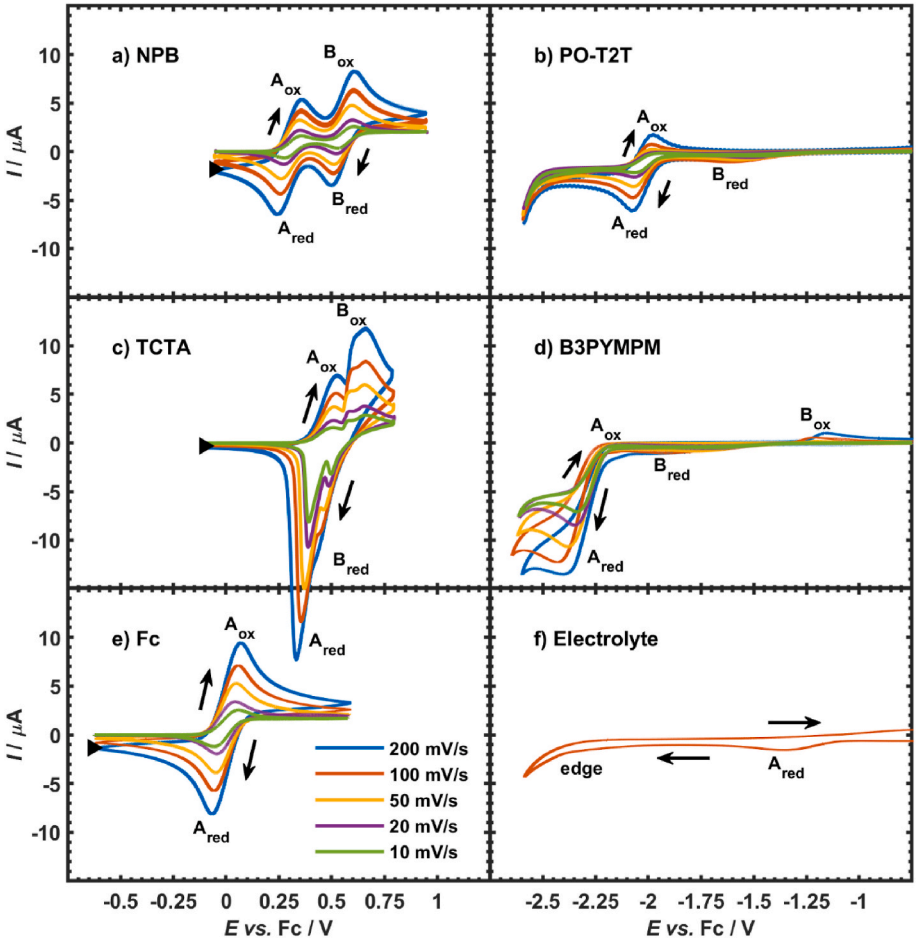

Fig. 4. CVs of $1x10^{-3}$ mol L^{-1} of NPB (a), PO-T2T (b), TCTA (c), B3PYMPM (d) and ferrocene (e) in dichloromethane with 0.1 mol L^{-1} TBAP as supporting electrolyte. Some non-critical data of (b), (d) and (f) were cut off and are provided in the ESI (Figs. S2, S6, S7). CVs for each compound were measured with scan rates between 10 mV s^{-1} and 200 mV s^{-1}. A CV of the supporting electrolyte measured at 100 mV s^{-1} is also included (f). The scan start and scan direction are indicated by the black triangles and the additional arrows. The labels (A_{ox}, A_{red} and B_{ox}, B_{red}) highlight the observed oxidation and reduction peaks. The reference potentials were normalized to the Fc redox potential, which was measured by addition of a small amount of ferrocene to each experiment (see Figures S2-4 and S6-7).

shown in Fig. 2a, the potential shift introduced due to handling of the setup (ΔE) must be considered. In Fig. 2b, $A_{ox}^{Ag\ QRE}$ has shifted from 0.908 V (Fig. 2a) to 0.926 V. The shift in A_{ox} is described by Equation (3) and amounts to $\Delta E = 0.018$ V for the example in Fig. 2.

$$\Delta E = A_{ox}^{Ag\ QRE}(\text{NPB with Fc exp}) - A_{ox}^{Ag\ QRE}(\text{NPB only exp}) \qquad \text{Equation 3}$$

To calculate the potential of the NPB only scan against the ferrocene scale (potential scale at the top of Fig. 2a), Equation (4) is used. A_{ox} can then be determined *vs.* Fc and is $A_{ox}^{Fc}(\text{NPB}) = 0.352$ V.

$$E_{\text{NPB only}}^{Fc} = E^{Ag\ QRE} - E_{redox}^{Ag\ QRE}(\text{Fc}) + \Delta E \qquad \text{Equation 4}$$

3.2. Determining HOMO an LUMO from electrochemistry

Electrochemical oxidation and reduction peaks originate from a single redox potential (E_{redox}) of the investigated molecules that are in contact with the working electrode, *i.e.,* one energy level such as a HOMO or a LUMO. The electrochemical peaks are spread out from this

central redox potential due to kinetic effects [37].

There are two methods to determine the redox potential for reversible or quasi-reversible systems: When both, the oxidation and the reduction peak are clearly visible, the redox potential (dashed line in Fig. 3a) is found half-way between the oxidation potential (E_{ox}) and the reduction potential (E_{red}), as described by Equation (5). This is the recommended method as it is the more accurate and more convenient method.

$$E_{redox} = \frac{E_{ox} + E_{red}}{2} \quad \text{Equation 5}$$

Alternatively, if only one peak can be observed properly, then E_{redox} can be determined from that peak only. This method is less accurate and leaves more room for interpretation, as it is more challenging to define the onset of a wave than it is to define a peak. However, it provides a method to analyze non-ideal systems. The redox potential for a reversible or quasi-reversible electrochemical system is approximately half-way between the peak potential (E_p) and the half-peak potential ($E_{p/2}$) which is the potential where the current is half of the peak current (I_p). There are two ways to determine the half-peak current $I_{p/2}$: i) In systems that show a flat (ohmic) region followed by the peak to be analyzed (such as NPB in Fig. 3), the peak- and half-peak current can be determined from the voltammogram after subtracting the background current obtained from a linear extrapolation of the flat region of the $I(E)$ curve (dotted line in Fig. 3b). ii) If the measured CV contains additional peaks in the region before the investigated peak, such as for B3PYMPM in Fig. 4d, a base current I_b can be chosen by eye, as illustrated in Fig. 3b, to find $I_{p/2}$ and I_p as given by equation (6) [37].

$$I_{p/2} = \frac{I_p + I_b}{2} \quad \text{Equation 6}$$

The redox potential of a single peak is then found at

$$E_{redox} = \frac{E_{p/2} + E_p}{2} \quad \text{Equation 7}$$

The difference in E_{HOMO} for NPB obtained using the two methods is approximately 10 mV as discussed in section 4.1.1, which is a typical error in electrochemical experiments.

3.3. Conversion from the electrochemical to the vacuum scale

Conversion of the energy levels from the electrochemical reference scale to the vacuum scale is discussed widely in the literature. Cardona and her co-workers provided a good overview over the complexity of the issue [41]. Briefly, the electrochemical potential scale (E *vs.* Fc/V) and the vacuum energy scale (E *vs.* vacuum/eV) are similar but have different zero points and are of opposite sign.

Conversion to the vacuum scale was achieved using Equation (8) where e denotes the elementary charge.

$$E(vs.\ \text{vacuum}\ /\ \text{eV}) = -(e \cdot E(vs.\ \text{Fc}\ /\ \text{V}) - (-4.99\ \text{eV})) \quad \text{Equation 8}$$

The conversion parameter of −4.99 eV corresponds to the redox potential of ferrocene *vs.* vacuum scale, taking the ferrocene redox potential as 0.31 V *vs.* SCE (= 0.55 V *vs.* SHE) [37] and the relationship between the electrochemical scale and the vacuum scale as 0 V *vs.* SHE = −4.44 eV *vs.* vacuum, as suggested by Trasatti [42]. Cardona used −5.1 eV as conversion parameter in Equation (8) [41], and it is very important to note, that this conversion parameter varies significantly between different sources [41]. This inconsistency, which originates from difficulties in determining various parameters, mandates that full transparency is provided when reporting the electrochemical characterization of semiconductor materials.

Equation (8) is valid for converting the energy levels measured in solution from the ferrocene scale to the vacuum scale. In actual OLED devices, the semiconductors are used as thin films, thus, it would be interesting to estimate the energy levels in films from solution measurements. The energy levels in films will, in general, change due to the different polarization of the molecules in thin films. Because the dipolar environment depends on the material and the film morphology, an accurate prediction is hardly possible. However, a linear relation between solution measurements and thin-film measurements has been described by multiple authors [20–23]. The energy levels in a thin film (E_{film}) can be estimated from the energy levels measured in solution ($E_{solution}$) via where the conversion parameters α and β are different for the HOMO (α^+,β^+) and the LUMO (α^-,β^-) level and vary depending on the materials and methods used to derive them (see e.g. Ref. [23]). Table S1 shows the values of the conversion parameters used below.

$$E_{film} = \alpha^{+/-} \cdot E_{solution} + \beta^{+/-} \quad \text{Equation 9}$$

Table 1
HOMO and LUMO energy levels of the OLED materials vs. the electrochemical ferrocene scale with experimental standard deviations (σ) and vs. the vacuum scale. The redox potential of ferrocene was taken as 0.55 V vs. SHE [37] and the vacuum conversion scale as 0 V vs. SHE = −4.44 eV [42]. The method used to calculate the potential from the experimental data is also indicated. The energy levels for thin films are estimated with the conversion parameters in Table S1.

	Frontier orbital	E *vs.* Fc (standard deviation)	Method	E *vs.* vacuum	Efilm *vs.* vacuum (difference)
NPB	HOMO	0.31 V (σ = 8 mV)	Eq. 5	−5.30 eV	−5.04 to −5.45 eV (Δ = 0.41)
		0.32 V (σ = 5 mV)	Eq. 7	−5.31 eV	−5.05 to −5.46 eV (Δ = 0.41)
TCTA	HOMO	0.483 V (σ = 5 mV)	Eq. 7	−5.47 eV	−5.28 to −5.66 eV (Δ = 0.38)
PO-T2T	LUMO	−2.03 V (σ = 10 mV)	Eq. 7	−2.96 eV	−2.36 to −2.43 eV (Δ = 0.07)
B3PYMPM	LUMO	−2.33 V (σ = 26 mV)	Eq. 7	−2.67 eV	−2.01 to −2.09 eV (Δ = 0.08)
	HOMO	1.20 V	Eq. 7	−6.19 eV	−6.17 to −6.55 eV (Δ = 0.38)

3.4. Discussion on the uncertainties

There are multiple sources of uncertainties associated with the presented electrochemical measurements, which we discuss in the following.

The potential is measured against a silver quasi-reference electrode. While the absolute potential of the silver wire can vary between two measurements, it is usually assumed to be stable within the time frame of an experiment. Because the potential of the quasi-reference electrode is calibrated against ferrocene, and ferrocene is assumed to be stable, there is a negligible uncertainty associated with the quasi-reference electrode. However, as mentioned in the context of eq. (3), the uncertainties due to handling the setup when adding ferrocene can be on the order of 20 mV, but by considering ΔE when calculating the potential with respect to the ferrocene scale, this source of error should be eliminated.

When the measured data does not show clear oxidation and reduction peaks, the preferred method of extracting the HOMO/LUMO potential (eq. (5)) cannot be used. Thus, an uncertainty occurs from the non-ideal method of determining the HOMO/LUMO potential. From the comparison of the two methods for NPB in section 4.1.1, a rough estimate of this uncertainty is on the order of 10 mV. Providing a general statement on the level of uncertainty is difficult, and it has to be assessed for each individual case.

Repeated measurements on the same material in the same cell can lead to different HOMO/LUMO levels. For the measurement presented

in section 4 we use the standard deviation to quantify these uncertainties, which are on the order of 10–30 mV (cf. Table 1).

As shown in Fig. S8, the scan rate also contributes to the uncertainty of the extracted HOMO/LUMO levels. The standard deviation of the measured energy levels varied between 8 mV and 26 mV, thus, the uncertainty from the scan rate might also be on the order of 10–30 mV.

When converting the potential from the ferrocene scale to the vacuum scale, we used a conversion parameter of −4.99 eV (cf. eq. (8)), while other authors used −5.1 eV as discussed in section 3.3. Since the true value of this conversion parameter is unknown, we can only speculate that the uncertainty will be on the order of 0–100 mV.

By adding up the described uncertainties, one arrives at typical uncertainties of ≈30–70 mV on the ferrocene scale and of ≈30–170 mV on the vacuum scale for the solution measurements. The estimated energy levels in thin films are listed in Table 1. Based on the large differences obtained from conversion parameters reported by different groups (cf. Table S1), an uncertainty of up to ≈400 mV for the HOMO and ≈100 mV for the LUMO has to be added for thin film energy levels. Considering that Kubo et al. used a more accurate technique than other groups, the uncertainty of determining the thin film HOMO might also be smaller.

4. Results and discussions

4.1. Voltammetric characterization

NPB, TCTA, PO-T2T and B3PYMPM were characterized using cyclic voltammetry. All measurements were started at or near the open-circuit potential, as measured with the potentiostat. The initial potential and the scan direction are indicated by a black triangle and arrows in the cyclic voltammograms (CVs) shown in Fig. 4. For the hole conductors NPB and TCTA, the potential was first swept towards the HOMO (in the positive, anodic direction), for the electron conductors PO-T2T and B3PYMPM it was first swept towards the LUMO (in the negative, cathodic direction). The scan direction was reversed once the electrochemical oxidation or reduction was observed. Scans were performed with three repeats to determine whether the conditions were stable. Scans were also recorded at a range of scan rates between 10 and 200 mV/s to gain more detailed insight into the electrochemical behavior as discussed below. Fig. 4 also presents cyclic voltammograms of the ferrocene standard redox couple (e) and of the electrochemical background containing only the electrolyte (f). Larger versions of these CVs, of CVs with added ferrocene, and some additional electrochemical analyses are provided in the ESI (Figs. S1–S7). For most of the investigated materials it was only possible to electrochemically observe one of the band edges since the other energy level was beyond the accessible potential window of the electrolyte (cf. Fig. S2).

4.1.1. NPB

NPB has two similar reversible peak pairs A and B (see Fig. 4a and Fig. S3) which have been previously observed [10,32–34]. The peaks do not shift significantly with changing scan rate (Fig. S3c) as expected, and the small fluctuations in the peak position of A_{ox} at different scan rates are similar to fluctuations of the "ideal" ferrocene (Fig. S1b), indicating a reversible electrochemical system. Another indication for a reversible peak pair is a peak-to-peak separation of approximately 59 mV [37], and although the peak-to-peak separation of 92 mV is significantly larger than the ideal 59 mV, this is normal for non-aqueous solvents [43]. In comparison, the average peak-to-peak separation measured for the ferrocene only experiment (Fig. 4e and Fig. S1) was 106 mV.

The first peak pair in Fig. 4a (A_{ox} – A_{red}) can be associated with the position of the HOMO and is probably caused by oxidation of one of the two symmetrical tertiary amine groups. The second peak pair (B_{ox} - B_{red}) can be associated with the HOMO+1 energy level. The peak current of B_{ox} was similar to the peak current of A_{ox}, suggesting that also the second reaction is a one-electron process. To compare the peak currents, A_{ox} was measured from the base of the peak (4.9 μA for 100 mV/s) and B_{ox} was measured from the dip between A_{ox} and B_{ox} (3.8 μA for 100 mV/s). This determination of the peak height is not very precise, because the onset of B_{ox} cannot be determined since A_{ox} obscures the true onset of B_{ox}. However, the ratio of A_{ox}:B_{ox} = 1:0.8 cannot account for a multi-electron process and the qualitative assessment holds firm.

Since CVs of NPB show relatively ideal reversible electrochemical behavior, the position of the HOMO of NPB can be directly determined from the redox potential of the A_{ox} – A_{red} peak pair using Equation (5). The redox potential was evaluated from 18 separate scans recorded at five different scan rates and for both, the NPB-only CVs and the NPB in the presence of ferrocene CVs (see ESI Figure S3). The redox potentials of NPB were then individually determined and averaged over all 36 measurements to yield a value of 0.311 V vs. Fc with a standard deviation (σ) of 8 mV. Using the second method (Equation (7)) to extract the redox potential, as discussed in section 3.2, the value is 0.321 V vs. Fc (σ = 5 mV) (see Fig. S8). After conversion to the vacuum scale using Equation (3), we obtain a HOMO energy level of −5.301 eV or −5.311 eV, respectively. This aligns well with literature values, where HOMO energy levels between −5.18 [33] and −5.7 eV [44,45] were reported. The HOMO+1 energy level was also assessed using the redox potential and was 0.564 V vs. Fc (σ = 12 mV), or −5.55 eV.

4.1.2. TCTA

The first report of the hole transporter TCTA was by Shirota and co-workers [11]. The HOMO was reported as a solid-state ionization potential of 5.7 eV, without giving further experimental details. Many subsequent publications do not mention the origin of their energy level information and no electrochemical characterization was found.

The lack of electrochemical characterization may be associated with the more complex electrochemical behavior of TCTA. The CV of TCTA shown in Fig. 4c and Figs. S4–5 is clearly complex. The HOMO of TCTA can be associated with the A_{ox}, A_{red} peak pair. The oxidation peak A_{ox} appears reasonably reversible, as the peak current is proportional to the square root of the scan rate (see Fig. S4c) and the peak potential does not shift significantly with the scan rate (see Fig. S4d). The peak current is similar to the peak current measured for NPB or for ferrocene, suggesting a one-electron process. However, the reduction peak A_{red} does not fit well with A_{ox}. It is too large and too sharp to be simply caused by the reverse of the oxidation reaction. Instead, A_{red} is distorted by the more anodic peaks labelled as B_{ox} and B_{red} in Fig. 4c and in Figs. S4a and b. We note that the distortions remained when the potential was reversed just after A_{ox} and before the peak B_{ox} was reached. B_{ox} consists of two strongly overlapping oxidation peaks. The reverse peak B_{red} is strongly overlapped by A_{red}, especially at faster scan rates. The steep shape of B_{ox} and subsequently A_{red} indicates complex electrochemical behavior, likely associated with electrochemical deposition and stripping processes. This is supported by further electrochemical observations: If the potential window is increased to even more positive potentials, the cyclic voltammograms start changing significantly from scan to scan (Fig. S5), a further tell-tale sign of a changing electrode surface and electrodeposition. The electrodeposition process was confirmed by a visible deposit observed on the electrode surface after such an experiment, shown as insets in Fig. S5 and has also been reported in Ref. [46]. Therefore, the reduction peak should not be used for extracting the HOMO level.

As the reduction peak was not reliable, the potential of the HOMO was determined from the oxidation peak only. The HOMO (averaged over all 36 measurements) was 0.483 V vs. Fc (σ = 5 mV) (see Fig. S8), corresponding to a HOMO energy level of −5.473 eV in the vacuum scale. HOMO energy levels in the literature were reported between −5.09 eV [47] and −5.9 eV [48], agreeing well with our finding.

4.1.3. PO-T2T

Hung and co-workers who first reported on PO-T2T described the electrochemical behavior of the LUMO of the electron transporter PO-T2T as quasi-reversible [12]. CVs of PO-T2T are presented in Fig. 4b,

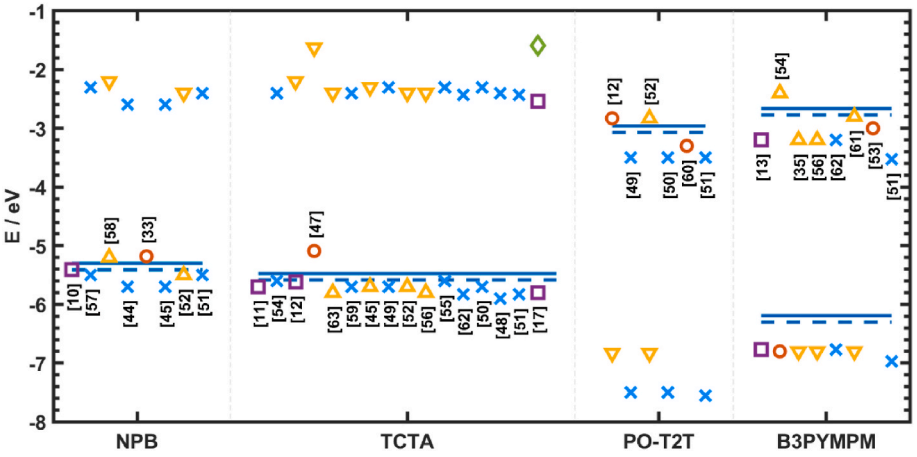

Fig. 5. Experimentally determined HOMO and LUMO energy levels for the four OLED materials in this work indicated by blue horizontal lines (solid lines were calculated using a conversion parameter of −4.99 eV, dashed lines with a conversion parameter of −5.1 eV). Energy levels found in the literature are also included with symbols [10–13,17,33,35,44,45,47–63], where yellow triangles represent HOMO and LUMO energy levels that were reported without or with inconclusive further referencing or experimental information, blue crosses represent energy levels that were reported with literature sources, purple squares represent data obtained from ionization potential measurements, the green diamond shows a result from low-energy inverse photoemission spectroscopy, and red circles represent data that were determined electrochemically.

with a larger version of the CVs provided in the supplementary information (Fig. S6). A tiny peak pair (B_{red}, B_{ox}) is followed by a second, more prominent peak pair (A_{red}, A_{ox}). The smaller peak pair (B_{red}, B_{ox}) at potentials near −1.6 V and −0.8 V is associated with electrochemical reactions of the platinum electrode. Similar peaks were also observed in the pure electrolyte (see Fig. S2) and no corresponding peaks were observed by Hung et al. who used a glassy carbon working electrode for their voltammetric characterization [12].

The LUMO level of PO-T2T is associated with the reduction peak of the main peak pair (A_{red}, A_{ox}). While the reaction of the main peaks is clearly not fully reversible, given the small oxidation peak, the reduction peak nevertheless shows relatively reversible behavior. The oxidation peak (A_{ox}) was only weak and disappears for slow scan rates. Even at the faster scan rates the oxidation currents only corresponded to approximately 15% of the reduction currents. Judging solely on the reversibility of the main peak pair, one might mistakenly conclude that PO-T2T is not a good semiconductor, despite its proven use in OLEDs. This effect is even more pronounced in B3PYMPM as discussed below.

The peak current of A_{red} scales linearly with the square root of the scan rate (cf. Fig. S6c) and the peak potential is not strongly dependent on the scan rate (see Fig. S6d). The magnitudes of the LUMO currents are similar to the currents measured for the HOMO peaks of the hole conductors and ferrocene, suggesting that also this process is a one-electron reaction.

The position of the LUMO of PO-T2T was determined from the reduction peaks of the 36 data sets analogous to the method used for TCTA and was −2.032 V (σ = 8 mV) (see Fig. S8). The corresponding LUMO level in the vacuum scale is thus −2.958 eV, agreeing well with the literature, where LUMO levels between −3.5 eV [49–51] and −2.83 eV [12,52] have been reported.

4.1.4. B3PYMPM

On first inspection, B3PYMPM shows similar electrochemical behavior to PO-T2T (see Fig. 4d). A large main signal (A_{red}, A_{ox}) is preceded by a small peak pair (B_{red}, B_{ox}), which can be associated with the platinum surface (see Fig. S3 and section 4.1.3). However, compared to PO-T2T, the main redox peak pair (A_{red},A_{ox}) is not behaving in a reversible manner, with the peak reduction potential shifting clearly as a function of the scan rate (cf. Fig. 4d and S7e) and the peak current not being linearly dependent on the square root of the scan rate (Fig. S7d). A_{ox} is fully suppressed for fast scan rates and only appears very tentatively for slow scan rates. It is interesting, that for an electron conductor material the electrochemical electron extraction is completely absent. If the electron injection were indeed not reversible at all, the available material in a device would quickly be used up and the device would stop working. Most likely, the lack of an electrochemical oxidation peak cannot be directly related to the solid-state behavior of B3PYMPM. Thus, care must be taken when judging the quality of a potential OLED material solely from its electrochemical behavior.

Another notable observation is that the reduction peak associated with the LUMO is extremely large. The observed currents are approximately double the currents observed for the other materials, despite the concentration being nominally equal. This suggests that the number of transferred electrons in the reaction may be two, possibly because the LUMO and the LUMO+1 are energetically very close together so that the electrochemical signals overlap. However, further investigations would be needed to confirm this.

The LUMO of B3PYMPM was again determined from the reduction peak only and was at −2.325 V vs. Fc (σ = 26 mV) (see Fig. S8). On the vacuum scale this gives a LUMO energy level of −2.665 eV. A broad range of LUMO levels have been reported in literature, ranging from −2.4 eV to −3.53 eV [13,35,51,53,54].

B3PYMPM was the only material we investigated where the LUMO and the HOMO are within the electrochemical window of the electrolyte. In the literature, one report was found where the HOMO energy level was determined from a very small, irreversible oxidation peak in the CV [35]. We could also access the HOMO of B3PYMPM (see Fig. S7c). The very small oxidation peak suggests a HOMO potential of 1.2 V vs. Fc, corresponding to a HOMO energy level of −6.19 eV in the vacuum scale. The oxidation peak associated with the HOMO was not stable in subsequent scans and was thus not further investigated.

4.2. Comparing energy levels to literature values

The electrochemically determined HOMO and LUMO energy levels are summarized in Table 1 together with the energy levels estimated for thin films from Equation (9) using the conversion parameters listed in Table S1. A visual representation of the electrochemical potentials and the energy levels in the vacuum scale as a function of the scan rate is further provided in the supporting information (Fig. S8). The electrochemical HOMO or LUMO potentials *vs.* ferrocene and the energies *vs.* the vacuum scale are provided together with information about the ferrocene redox potential *vs.* SHE and the vacuum conversion scale. Providing these data is necessary to make electrochemical studies comparable.

In Fig. 5 the electrochemically determined HOMO and LUMO energy levels of the OLED materials are compared to values found in the literature [10–13,33,35,44,45,47–63]. The literature values are from electrochemical measurements in solution, from measurements on thin films using different techniques, or from other sources as indicated with the markers. Fig. 5 shows that the electrochemically determined HOMO and LUMO energy levels presented in this report compare well with the literature data, independent of how the energy levels were determined. What is most striking about the figure is that there are sometimes very

large differences between the cited energy levels for the different materials and that in many publications it is not entirely clear how the information about the energy levels was obtained. This discrepancy clearly underlines the relevance of the present work and for a unified approach to energy level determination.

5. Conclusions

This paper presents an easy-to-follow method for the determination of frontier orbital energy levels of small molecular organic semiconductors from cyclic voltammetry measurements in solution. The presented analysis of the cyclic voltammograms allows the evaluation of non-ideal CVs and describes the conversion from the electrochemical to the vacuum energy scale for the HOMO and LUMO energy levels. The measured HOMO and LUMO energy levels of the four investigated OLED materials correspond well with literature values. Even though the energy levels are not measured in the same dipolar environment as in the final device stack, we argue that cyclic voltammetry measurements in solution yield fairly accurate estimations of the energy levels, especially since the spread in existing literature data is rather large. The presented method should support and motivate future studies to perform cyclic voltammetry measurements on a regular basis to provide more accurate HOMO and LUMO energy levels.

Declaration of competing interest

The authors declare that they have no known competing financial interests or personal relationships that could have appeared to influence the work reported in this paper.

Data availability

Data will be made available on request.

6. Acknowledgements

The authors thank Dr. Evelyne Knapp and Dr. Sevki Cevher from ZHAW for fruitful discussions. Financial support from the Swiss National Science Foundation under grant no. 182624 is gratefully appreciated.

Appendix A. Supplementary data

Supplementary data to this article can be found online at https://doi.org/10.1016/j.orgel.2023.106888.

References

[1] G. Hong, X. Gan, C. Leonhardt, Z. Zhang, J. Seibert, J.M. Busch, S. Bräse, A brief history of OLEDs—emitter development and industry milestones, Adv. Mater. 33 (2021), 2005630, https://doi.org/10.1002/adma.202005630.
[2] M. Regnat, C.-K. Moon, S. Jenatsch, B. Ruhstaller, K.P. Pernstich, Pinpointing the origin of the increased driving voltage during prolonged operation in a phosphorescent OLED based on an exciplex host, Org. Electron. 108 (2022), 106570, https://doi.org/10.1016/j.orgel.2022.106570.
[3] M. Neukom, S. Züfle, S. Jenatsch, B. Ruhstaller, Opto-electronic characterization of third-generation solar cells, Sci. Technol. Adv. Mater. 19 (2018) 291–316, https://doi.org/10.1080/14686996.2018.1442091.
[4] J.C. Scott, Metal–organic interface and charge injection in organic electronic devices, J. Vac. Sci. Technol. A 21 (2003) 521–531, https://doi.org/10.1116/1.1559919.
[5] M. Jeong, J.F. Joung, J. Hwang, M. Han, C.W. Koh, D.H. Choi, S. Park, Deep learning for development of organic optoelectronic devices: efficient prescreening of hosts and emitters in deep-blue fluorescent OLEDs, npj Comput. Mater. 8 (2022) 1–11, https://doi.org/10.1038/s41524-022-00834-3.
[6] H. Gao, Theoretical investigation into charge mobility in 4,4′-bis(1-naphthylphenylamino)biphenyl, Theor. Chem. Acc. 127 (2010) 759–763, https://doi.org/10.1007/s00214-010-0804-9.
[7] B.C. Lin, C.P. Cheng, Z.P.M. Lao, Reorganization energies in the transports of holes and electrons in organic amines in organic electroluminescence studied by density functional theory, J. Phys. Chem. 107 (2003) 5241–5251, https://doi.org/10.1021/jp0304529.
[8] S. Alam, V. Nádaždy, T. Váry, C. Friebe, R. Meitzner, J. Ahner, A. Anand, S. Karuthedath, C.S.P.D. Castro, C. Göhler, S. Dietz, J. Cann, C. Kästner, A. Konkin, W. Beenken, A.M. Anton, C. Ulbricht, A. Sperlich, M.D. Hager, U. Ritter, F. Kremer, O. Brüggemann, U.S. Schubert, D.A.M. Egbe, G.C. Welch, V. Dyakonov, C. Deibel, F. Laquai, H. Hoppe, Uphill and downhill charge generation from charge transfer to charge separated states in organic solar cells, J. Mater. Chem. C 9 (2021) 14463–14489, https://doi.org/10.1039/D1TC02351A.
[9] C.S. Fadley, X-ray photoelectron spectroscopy: from origins to future directions, Nucl. Instrum. 601 (2009) 8–31, https://doi.org/10.1016/j.nima.2008.12.189.
[10] L.-B. Lin, M.G. Mason, R.H. Young, D.E. Schildkraut, P.M. Borsenberger, S. A. Jenekhe, Investigation of organic-organic interfaces by time-resolved photocurrent, electrochemical, and photoemission techniques, MRS Online Proc. Libr. 488 (1997) 689–693, https://doi.org/10.1557/PROC-488-689.
[11] Y. Kuwabara, H. Ogawa, H. Inada, N. Noma, Y. Shirota, Thermally stable multilared organic electroluminescent devices using novel starburst molecules, 4,4′,4″-Tri(N-carbazolyl)triphenylamine (TCTA) and 4,4′,4″-Tris(3-methylphenylphenylamino)triphenylamine (m-MTDATA), as hole-transport materials, Adv. Mater. 6 (1994) 677–679, https://doi.org/10.1002/adma.19940060913.
[12] W.-Y. Hung, G.-C. Fang, S.-W. Lin, S.-H. Cheng, K.-T. Wong, T.-Y. Kuo, P.-T. Chou, The first tandem, all-exciplex-based WOLED, Sci. Rep. 4 (2014) 5161, https://doi.org/10.1038/srep05161.
[13] D. Tanaka, H. Sasabe, Y.-J. Li, S.-J. Su, T. Takeda, J. Kido, Ultra high efficiency green organic light-emitting devices, Jpn. J. Appl. Phys. 46 (2007) L10–L12, https://doi.org/10.1143/JJAP.46.L10.
[14] I.G. Hill, A. Kahn, Z.G. Soos, R.A. Pascal Jr., Charge-separation energy in films of π-conjugated organic molecules, Chem. Phys. Lett. 327 (2000) 181–188, https://doi.org/10.1016/S0009-2614(00)00882-4.
[15] C.I. Wu, Y. Hirose, H. Sirringhaus, A. Kahn, Electron-hole interaction energy in the organic molecular semiconductor PTCDA, Chem. Phys. Lett. 272 (1997) 43–47, https://doi.org/10.1016/S0009-2614(97)00481-8.
[16] H. Yoshida, Principle and application of low energy inverse photoemission spectroscopy: a new method for measuring unoccupied states of organic semiconductors, J. Electron. Spectrosc. Relat. Phenom. 204 (2015) 116–124, https://doi.org/10.1016/j.elspec.2015.07.003.
[17] H. Yoshida, K. Yoshizaki, Electron affinities of organic materials used for organic light-emitting diodes: a low-energy inverse photoemission study, Org. Electron. 20 (2015) 24–30, https://doi.org/10.1016/j.orgel.2015.01.037.
[18] V. Palermo, M. Palma, P. Samorì, Electronic characterization of organic thin films by kelvin probe force microscopy, Adv. Mater. 18 (2006) 145–164, https://doi.org/10.1002/adma.200501394.
[19] X. Zhou, J. Zhang, G. Bai, C. Wang, W. He, X. Sun, J. Zhang, J. Miao, A novel energy level detector for molecular semiconductors, Phys. Chem. Chem. Phys. 24 (2022) 2717–2728, https://doi.org/10.1039/D1CP01842F.
[20] B.W. D'Andrade, S. Datta, S.R. Forrest, P. Djurovich, E. Polikarpov, M. E. Thompson, Relationship between the ionization and oxidation potentials of molecular organic semiconductors, Org. Electron. 6 (2005) 11–20, https://doi.org/10.1016/j.orgel.2005.01.002.
[21] P.I. Djurovich, E.I. Mayo, S.R. Forrest, M.E. Thompson, Measurement of the lowest unoccupied molecular orbital energies of molecular organic semiconductors, Org. Electron. 10 (2009) 515–520, https://doi.org/10.1016/j.orgel.2008.12.011.
[22] J. Sworakowski, J. Lipinski, K. Janus, On the reliability of determination of energies of HOMO and LUMO levels in organic semiconductors from electrochemical measurements. A simple picture based on the electrostatic model, Org. Electron. 33 (2016) 300–310, https://doi.org/10.1016/j.orgel.2016.03.031.
[23] M. Kubo, H. Yoshida, Electron affinities of small-molecule organic semiconductors: comparison among cyclic voltammetry, conventional inverse photoelectron spectroscopy, and low-energy inverse photoelectron spectroscopy, Org. Electron. 108 (2022), 106551, https://doi.org/10.1016/j.orgel.2022.106551.
[24] V. Nádaždy, F. Schauer, K. Gmucová, Energy resolved electrochemical impedance spectroscopy for electronic structure mapping in organic semiconductors, Appl. Phys. Lett. 105 (2014), 142109, https://doi.org/10.1063/1.4898068.
[25] H. Bässler, D. Kroh, F. Schauer, V. Nádaždy, A. Köhler, Mapping the density of states distribution of organic semiconductors by employing energy resolved–electrochemical impedance spectroscopy, Adv. Funct. Mater. 31 (2021), 2007738, https://doi.org/10.1002/adfm.202007738.
[26] K. Gmucová, V. Nádaždy, F. Schauer, M. Kaiser, E. Majková, Electrochemical spectroscopic methods for the fine band gap electronic structure mapping in organic semiconductors, J. Phys. Chem. C 119 (2015) 15926–15934, https://doi.org/10.1021/acs.jpcc.5b04378.
[27] F. Schauer, V. Nádaždy, K. Gmucová, Electrochemical impedance spectroscopy for study of electronic structure in disordered organic semiconductors—possibilities and limitations, J. Appl. Phys. 123 (2018), 161590, https://doi.org/10.1063/1.5008830.
[28] P. Acevedo-Peña, A. Baray-Calderón, H. Hu, I. González, V.M. Ugalde-Saldivar, Measurements of HOMO-LUMO levels of poly(3-hexylthiophene) thin films by a simple electrochemical method, J. Solid State Electrochem. 21 (2017) 2407–2414, https://doi.org/10.1007/s10008-017-3587-2.
[29] J. García-Cañadas, F. Fabregat-Santiago, H.J. Bolink, E. Palomares, G. Garcia-Belmonte, J. Bisquert, Determination of electron and hole energy levels in mesoporous nanocrystalline TiO2 solid-state dye solar cell, Synth. Met. 156 (2006) 944–948, https://doi.org/10.1016/j.synthmet.2006.06.006.
[30] L. Leonat, G. Sbârcea, I.V. Brânzoi, Cyclic voltammetry for energy levels estimation of organic materials, U.P.B. Sci. Bull., Series B. 75 (2013) 111–118. https://www.scientificbulletin.upb.ro/rev_docs_arhiva/rezdd1_869282.pdf.

[31] K.A. Bogdanowicz, B. Jewłoszewicz, A. Iwan, K. Dysz, W. Przybyl, A. Januszko, M. Marzec, K. Cichy, K. Świerczek, L. Kavan, M. Zukalová, V. Nadazdy, R. Subair, E. Majkova, M. Micusik, M. Omastova, M.D. Özeren, K. Kamarás, D.Y. Heo, S. Y. Kim, Selected electrochemical properties of 4,4'-((1E,1'E)-((1,2,4-Thiadiazole-3,5-diyl)bis(azaneylylidene))bis(methaneylylidene))bis(N,N-di-p-tolylaniline) towards perovskite solar cells with 14.4% efficiency, Materials 13 (2020) 2440, https://doi.org/10.3390/ma13112440.
[32] S.A. Van Slyke, C.H. Chen, C.W. Tang, Organic electroluminescent devices with improved stability, Appl. Phys. Lett. 69 (1996) 2160–2162, https://doi.org/10.1063/1.117151.
[33] J.-E. Park, S. Song, I.-S. Shin, Voltammetric investigation for electron-transfer characteristics of organic semiconductors, Int. J. Electrochem. Sci. 11 (2016) 5891–5899, https://doi.org/10.20964/2016.07.14.
[34] R. Fáber, G.F. Mielke, P. Rapta, A. Staško, O. Nuyken, Anodic oxidation of novel hole-transporting materials derived from tetraarylbenzidines. Electrochemical and spectroscopic characterization, Collect. Czech Chem. Commun. 65 (2000) 1403–1418, https://doi.org/10.1135/cccc20001403.
[35] S.-F. Wu, S.-H. Li, Y.-K. Wang, C.-C. Huang, Q. Sun, J.-J. Liang, L.-S. Liao, M.-K. Fung, White organic LED with a luminous efficacy exceeding 100 lm W−1 without light out-coupling enhancement techniques, Adv. Funct. Mater. 27 (2017), 1701314, https://doi.org/10.1002/adfm.201701314.
[36] N. Elgrishi, K.J. Rountree, B.D. McCarthy, E.S. Rountree, T.T. Eisenhart, J. L. Dempsey, A practical beginner's guide to cyclic voltammetry, J. Chem. Educ. 95 (2018) 197–206, https://doi.org/10.1021/acs.jchemed.7b00361.
[37] A.J. Bard, L.R. Faulkner, Electrochemical Methods: Fundamentals and Applications, second ed., John Wiley & Sons, Inc., 2020.
[38] Y. Takebayashi, N. Morii, K. Sue, T. Furuya, S. Yoda, D. Ikemizu, H. Taka, Solubility of N,N′-Di(1-naphthyl)-N,N′-diphenyl benzidine (NPB) in various organic solvents: measurement and correlation with the hansen solubility parameter, Ind. Eng. Chem. Res. 54 (2015) 8801–8808, https://doi.org/10.1021/acs.iecr.5b01219.
[39] G. Inzelt, A. Lewenstam, F. Scholz (Eds.), Handbook of Reference Electrodes, Springer, Berlin, Heidelberg, 2013, https://doi.org/10.1007/978-3-642-36188-3_1.
[40] G. Gritzner, J. Kuta, Recommendations on reporting electrode potentials in nonaqueous solvents (Recommendations 1983), Pure Appl. Chem. 56 (1984) 461–466, https://doi.org/10.1351/pac198456040461.
[41] C.M. Cardona, W. Li, A.E. Kaifer, D. Stockdale, G.C. Bazan, Electrochemical considerations for determining absolute frontier orbital energy levels of conjugated polymers for solar cell applications, Adv. Mater. 23 (2011) 2367–2371, https://doi.org/10.1002/adma.201004554.
[42] S. Trasatti, The absolute electrode potential: an explanatory note (Recommendations 1986), Pure Appl. Chem. 58 (1986) 955–966, https://doi.org/10.1351/pac198658070955.
[43] N.G. Tsierkezos, Cyclic voltammetric studies of ferrocene in nonaqueous solvents in the temperature range from 248.15 to 298.15 K, J. Solut. Chem. 36 (2007) 289–302, https://doi.org/10.1007/s10953-006-9119-9.
[44] J. Xu, Y. Wang, Q. Chen, Y. Lin, H. Shan, V.A.L. Roy, Z. Xu, Enhanced lifetime of organic light-emitting diodes using soluble tetraalkyl-substituted copper phthalocyanines as anode buffer layers, J. Mater. Chem. C 4 (2016) 7377–7382, https://doi.org/10.1039/C6TC01864E.
[45] F. Zhao, D. Ma, Approaches to high performance white organic light-emitting diodes for general lighting, Mater. Chem. Front. 1 (2017) 1933–1950, https://doi.org/10.1039/C6QM00365F.
[46] C. Zhao, Z. Chen, W. Wang, P. Xiong, B. Li, M. Li, J. Yang, Y. Xu, In situ electropolymerization enables ultrafast long cycle life and high-voltage organic cathodes for lithium batteries, Angew. Chem. Int. Ed. 59 (2020) 11992–11998, https://doi.org/10.1002/anie.202000566.
[47] B. Pan, H. Huang, X. Yang, J. Jin, S. Zhuang, G. Mu, L. Wang, Systematic study of TCTA-based star-shaped host materials by optimizing ratio of carbazole/diphenylphosphine oxide: achieving both low efficiency roll-off and turn-on voltage for blue PHOLEDs, J. Mater. Chem. C 2 (2014) 7428–7435, https://doi.org/10.1039/C4TC00951G.
[48] M. Regnat, K.P. Pernstich, K.-H. Kim, J.-J. Kim, F. Nüesch, B. Ruhstaller, Routes for efficiency enhancement in fluorescent TADF exciplex host OLEDs gained from an electro-optical device model, Adv. Electron. Mater. 6 (2020), 1900804, https://doi.org/10.1002/aelm.201900804.
[49] S. Ying, J. Yao, Y. Chen, D. Ma, High efficiency (~100 lm/W) hybrid WOLEDs by simply introducing ultrathin non-doped phosphorescent emitters in a blue exciplex host, J. Mater. Chem. C 6 (2018) 7070–7076, https://doi.org/10.1039/C8TC01736K.
[50] S. Ying, P. Pang, S. Zhang, Q. Sun, Y. Dai, X. Qiao, D. Yang, J. Chen, D. Ma, Superior efficiency and low-efficiency roll-off white organic light-emitting diodes based on multiple exciplexes as hosts matched to phosphor emitters, ACS Appl. Mater. Interfaces 11 (2019) 31078–31086, https://doi.org/10.1021/acsami.9b09429.
[51] Ossila, Ossila semiconducting molecules. https://www.ossila.com/collections/semiconducting-molecules. (Accessed 7 December 2021).
[52] G. Sych, J. Simokaitiene, O. Bezvikonnyi, U. Tsiko, D. Volyniuk, D. Gudeika, J. V. Grazulevicius, Exciplex-enhanced singlet emission efficiency of nondoped organic light emitting diodes based on derivatives of tetrafluorophenylcarbazole and tri/tetraphenylethylene exhibiting aggregation-induced emission enhancement, J. Phys. Chem. C 122 (2018) 14827–14837, https://doi.org/10.1021/acs.jpcc.8b03895.
[53] J. Zhao, X. Du, S. Yuan, C. Zheng, H. Lin, S. Tao, Highly efficient green and red OLEDs based on a new exciplex system with simple structures, Org. Electron. 43 (2017) 136–141, https://doi.org/10.1016/j.orgel.2017.01.020.
[54] A. Perumal, H. Faber, N. Yaacobi-Gross, P. Pattanasattayavong, C. Burgess, S. Jha, M.A. McLachlan, P.N. Stavrinou, T.D. Anthopoulos, D.D.C. Bradley, High-efficiency, solution-processed, multilayer phosphorescent organic light-emitting diodes with a copper thiocyanate hole-injection/hole-transport layer, Adv. Mater. 27 (2015) 93–100, https://doi.org/10.1002/adma.201403914.
[55] M. Regnat, K.P. Pernstich, B. Ruhstaller, Influence of the bias-dependent emission zone on exciton quenching and OLED efficiency, Org. Electron. 70 (2019) 219–226, https://doi.org/10.1016/j.orgel.2019.04.027.
[56] S.-H. Li, S.-F. Wu, Y.-K. Wang, J.-J. Liang, Q. Sun, C.-C. Huang, J.-C. Wu, L.-S. Liao, M.-K. Fung, Management of excitons for highly efficient organic light-emitting diodes with reduced triplet exciton quenching: synergistic effects of exciplex and quantum well structure, J. Mater. Chem. C 6 (2018) 342–349, https://doi.org/10.1039/C7TC04441K.
[57] E.W. Forsythe, M.A. Abkowitz, Y. Gao, C.W. Tang, Influence of copper phthalocynanine on the charge injection and growth modes for organic light emitting diodes, J. Vac. Sci. Technol. A 18 (2000) 1869–1874, https://doi.org/10.1116/1.582438.
[58] N.H. Kim, Y.-H. Kim, J.-A. Yoon, S.Y. Lee, D.H. Ryu, R. Wood, C.-B. Moon, W. Y. Kim, Color optimization of single emissive white OLEDs via energy transfer between RGB fluorescent dopants, J. Lumin. 143 (2013) 723–728, https://doi.org/10.1016/j.jlumin.2013.05.048.
[59] Y. Li, L. Zhou, R. Cui, Y. Jiang, X. Zhao, W. Liu, Q. Zhu, Y. Cui, H. Zhang, High performance red organic electroluminescent devices based on a trivalent iridium complex with stepwise energy levels, RSC Adv. 6 (2016) 71282–71286, https://doi.org/10.1039/C6RA16517F.
[60] X.-K. Liu, Z. Chen, J. Qing, W.-J. Zhang, B. Wu, H.L. Tam, F. Zhu, X.-H. Zhang, C.-S. Lee, Remanagement of singlet and triplet excitons in single-emissive-layer hybrid white organic light-emitting devices using thermally activated delayed fluorescent blue exciplex, Adv. Mater. 27 (2015) 7079–7085, https://doi.org/10.1002/adma.201502897.
[61] M. Wang, Y.-H. Huang, K.-S. Lin, T.-H. Yeh, J. Duan, T.-Y. Ko, S.-W. Liu, K.-T. Wong, B. Hu, Revealing the cooperative relationship between spin, energy, and polarization parameters toward developing high-efficiency exciplex light-emitting diodes, Adv. Mater. 31 (2019), 1904114, https://doi.org/10.1002/adma.201904114.
[62] Q. Wang, Q.-S. Tian, Y.-L. Zhang, X. Tang, L.-S. Liao, High-efficiency organic light-emitting diodes with exciplex hosts, J. Mater. Chem. C 7 (2019) 11329–11360, https://doi.org/10.1039/c9tc03092a.
[63] S. Wu, S. Li, Q. Sun, C. Huang, M.-K. Fung, Highly efficient white organic light-emitting diodes with ultrathin emissive layers and a spacer-free structure, Sci. Rep. 6 (2016), 25821, https://doi.org/10.1038/srep25821.